Title

Assessment of multiple ecosystem metabolism methods in an estuary

Journal

Limnology and Oceanography: Methods, 19(11)

ISSN

1541-5856

Authors

Loken, LC
Van Nieuwenhuyse, EE
Dahlgren, RA
et al.

Publication Date

2021-11-01

DOI

10.1002/lom3.10458

Peer reviewed

LIMNOLOGY
and
OCEANOGRAPHY: METHODS

ASLO

Limnol. Oceanogr.: Methods 2021

doi: 10.1002/lom3.10458

Assessment of multiple ecosystem metabolism methods in an estuary

Luke C. Loken,[1,2]* **Erwin E. Van Nieuwenhuyse**,[3] **Randy A. Dahlgren**,[4] **Leah E. K. Lenoch**,[5] **Paul R. Stumpner**,[5] **Jon R. Burau**,[5] **Steven Sadro**[2]

[1]U.S. Geological Survey, Upper Midwest Water Science Center, Middleton, Wisconsin
[2]Department of Environmental Science and Policy, University of California-Davis, Davis, California
[3]Bureau of Reclamation, Science Division, Bay-Delta Office, Sacramento, California
[4]Department of Land, Air, and Water Resources, University of California-Davis, Davis, California
[5]U.S. Geological Survey, California Water Science Center, Sacramento, California

Abstract

Ecosystem metabolism is a key ecological attribute and easy to describe, but quantifying metabolism in estuaries is challenging. Properly scaling measurements through time and space requires consideration of hydrodynamics and mixing water from heterogeneous sources, making any estimation uncertain. Here, we compared three methods for modeling ecosystem metabolism in a portion of the Sacramento-San Joaquin Delta. Metabolism estimates based on laboratory incubations, continuous in situ buoys, and an oxygen isotope approach all indicated the system was net heterotrophic, and calculated rates were comparable in magnitude when averaged over the 2-month study. Daily metabolic rates based on in situ buoys were the most variable, likely due to horizontal and vertical advection and poor portrayal of the dissolved oxygen budget. After temporally averaging in situ buoy estimates or smoothing the dissolved oxygen time series for tidal effects, rates were more comparable to the other methods, which may be necessary to account for tidal advection and unbalanced contributions from subhabitats within the metabolic footprint. Incubation-based rates represent the finest temporal and spatial scale and only account for pelagic processes, which may explain why incubation-based rates were lower than the other two methods. The oxygen isotope method provided temporally and spatially integrated rates that were bracketed by the other two methods and may be a valuable tool in systems matching the model requirements. Because uncertainty arises in each method from a number of assumptions and scaling calculations, the resolution of metabolic rates in estuaries is likely coarser and more variable than in other aquatic ecosystems.

Ecosystem metabolism is a key ecological attribute describing the total amount of energy flowing through an ecosystem and its food web. Metabolism has been foundational in the development of ecosystem science and food web ecology (Lindeman 1942) and has implications for global carbon budgets and climate change (Cole et al. 2007; Yvon-Durocher et al. 2010). Generally, metabolism is separated into two components, gross primary production (GPP) and ecosystem respiration (ER), representing the production and consumption of organic carbon. Newly produced organic carbon (through GPP) supports the majority of the global food web, and in aquatic ecosystems represents the amount of new energy captured by phytoplankton, macrophytes, and other photosynthetic organisms. As organic carbon is consumed (through ER), energy is used for growth, movement, reproduction, and the myriad of biological processes within autotrophic and heterotrophic organisms. The balance between GPP and ER is net ecosystem production (NEP), noting whether the system is a net source or sink of organic carbon. Direct measurements of ecosystem metabolic rates have been made across aquatic ecosystems, including lakes, streams, rivers, estuaries, and the ocean (Caffrey 2004; Solomon et al. 2013; Demars et al. 2015; Yang et al. 2017). Many inland waters are net heterotrophic as they receive and respire surplus organic carbon from upstream ecosystems and terrestrial watersheds (Cole et al. 2007; Hoellein et al. 2013). However, a number of aquatic ecosystems, including many estuaries, are net autotrophic (Balmer and Downing 2011; Hoellein et al. 2013; Pacheco et al. 2014) as they produce more organic carbon than they respire, and thus either accumulate organic matter (e.g., blue carbon), stored in sediments or biomass, or export it to downstream rivers, lakes, or the ocean.

Our understanding of variation in metabolic rates through space or time across different types of aquatic ecosystems comes from nearly a century of measurements made using a

*Correspondence: lloken@usgs.gov

Additional Supporting Information may be found in the online version of this article.

variety of techniques (Staehr et al. 2012). Chemical measurements of changes in dissolved oxygen (DO) or inorganic carbon in light/dark bottle incubations have long been used to quantify metabolic rates (Gaarder and Gran 1927; Kemp et al. 1997; Gazeau et al. 2005). The development of the carbon isotope (^{14}C) uptake method provided a more direct and sensitive measurement of GPP (Steemann Nielsen 1952), though it retained the limitations of bottle incubations, including scale (Gerhart and Likens 1975). Something closer to ecosystem scale measurements was introduced with the application of the in situ mass balance approach, where diel variation in DO concentrations were used to model metabolic rates (Sargent and Austin 1949; Odum 1956). Several approaches relying on the measurement of oxygen isotopes (^{18}O) now provide both bottle and ecosystem scale estimates of metabolic rates (Grande et al. 1989; Hotchkiss and Hall 2014; Bogard et al. 2017). Each of the methods for quantifying ecosystem metabolic rates has different advantages and disadvantages, capturing slightly different spatial or temporal aspects of metabolic activity (Staehr et al. 2010). Although a variety of techniques have been applied across a range of aquatic ecosystems, few studies compared multiple approaches concurrently (Bott et al. 1978; Grande et al. 1989; Gazeau et al. 2005; Song et al. 2016; Murrell et al. 2018; Howard et al. 2020). Such studies allow for the direct comparison of metabolic rates and their variability. Moreover, they provide valuable insight into the efficacy of different approaches when making comparisons across ecosystems (Cloern et al. 2014), or when evaluating temporal or spatial variability within individual ecosystems with complex dynamics and habitat heterogeneity.

Estuaries are among the most challenging ecosystems in which to measure metabolic rates (Cloern et al. 2014) given their hydrodynamic complexity, habitat diversity, and steep biogeochemical and productivity gradients. Compared to lakes and rivers, estuaries do not have clear ecosystem boundaries and water depths can vary multiple meters within a daily tidal cycle. Habitat heterogeneity, channel geomorphometry, and tidal hydrodynamics create gradients or complex mosaics of water residence time, nutrient concentrations, salinity, and water clarity/light availability that affect ecosystem metabolic rates (Staehr et al. 2016; Shen et al. 2019; Tassone and Bukaveckas 2019; Ganju et al. 2020; Cloern et al. 2020). Consequently, water and its metabolic signal at a single location within an estuary represent a dynamic integration of habitat types (Wang et al. 2018) that expand/contract at hourly to annual timescales in response to ebb/flood and spring/neap tide dynamics and to river hydrology (Kemp & Boynton, 1980). The spatial extent and metabolic footprint for a given measurement is difficult to define, and accounting for such complexity in coupled metabolism-hydrodynamic models is challenging, not easily generalizable, and often ignored. Metabolism at the whole-estuary scale integrates the metabolic signal of all distinct subhabitats and the fluxes among them (Crosswell et al. 2017), making it difficult to properly scale point measurements to the whole system. Coupling simple mass-balance models that incorporate continually changing physical dimensions of surface area, volume, and depth, with a basic understanding of hydrodynamics and spatial heterogeneity can provide useful estimates of metabolic rates; however, interpreting such rates on their own can be challenging.

Here, we evaluated ecosystem metabolic rates in a comparatively hydrologically simple portion of the Sacramento-San Joaquin Delta using three different but concurrently applied methodological approaches: continuous in situ measurements of DO from multiple depths (referred to as "buoy" in the text), laboratory light/dark bottle incubations of DO ("incubation"), and measurements of oxygen isotopes ("^{18}O"). Metabolism was monitored over a 2-month period at multiple locations arranged in a spatial network across a 7-km segment of a dead-end slough. Across the study, we measured temporal and spatial variation in hydrodynamics, nutrient concentrations, and water clarity, all of which may have contributed to variation in true metabolism, but also to variation in model uncertainty. Lacking a true measure of ecosystem metabolism, we show that by comparing estimates using multiple approaches over a spatial and temporal domain, we can better constrain metabolism in an estuary.

Materials and procedures

Site description

The Sacramento River Deep Water Ship Channel (DWSC) is located in Northern California and is part of the greater San Francisco Bay/Sacramento-San Joaquin Delta Estuary (Fig. 1). The DWSC is ~ 40-km long, is ~ 150-m wide, and has a mean depth of 7.5 m. The entire DWSC is tidal, where water levels fluctuate up to 2 m daily. At the northern terminus of the DWSC, a set of decommissioned locks connect the DWSC to the Sacramento River. Although some water leaks through the locks during periods of high river flow, net flows in the DWSC are minimal. Because the system has minimal off-channel habitat and lacks upstream water inputs, functionally, the DWSC resembles a large dead-end slough with a straight and homogeneous channel form (Feyrer et al. 2017). The channel is organized longitudinally, where the seaward (southerly) side of the channel exchanges with the greater Delta with every tidal cycle. Moving landward (northernly), tidal excursion lengths compress (Stumpner et al. 2020), and water becomes increasingly isolated (Gross et al. 2019). Turbidity and dissolved inorganic nitrogen (DIN) also decrease moving landward in accordance with dampening flow velocities (Morgan-King and Schoellhamer 2013) and increasing water residence time (Downing et al. 2016), respectively.

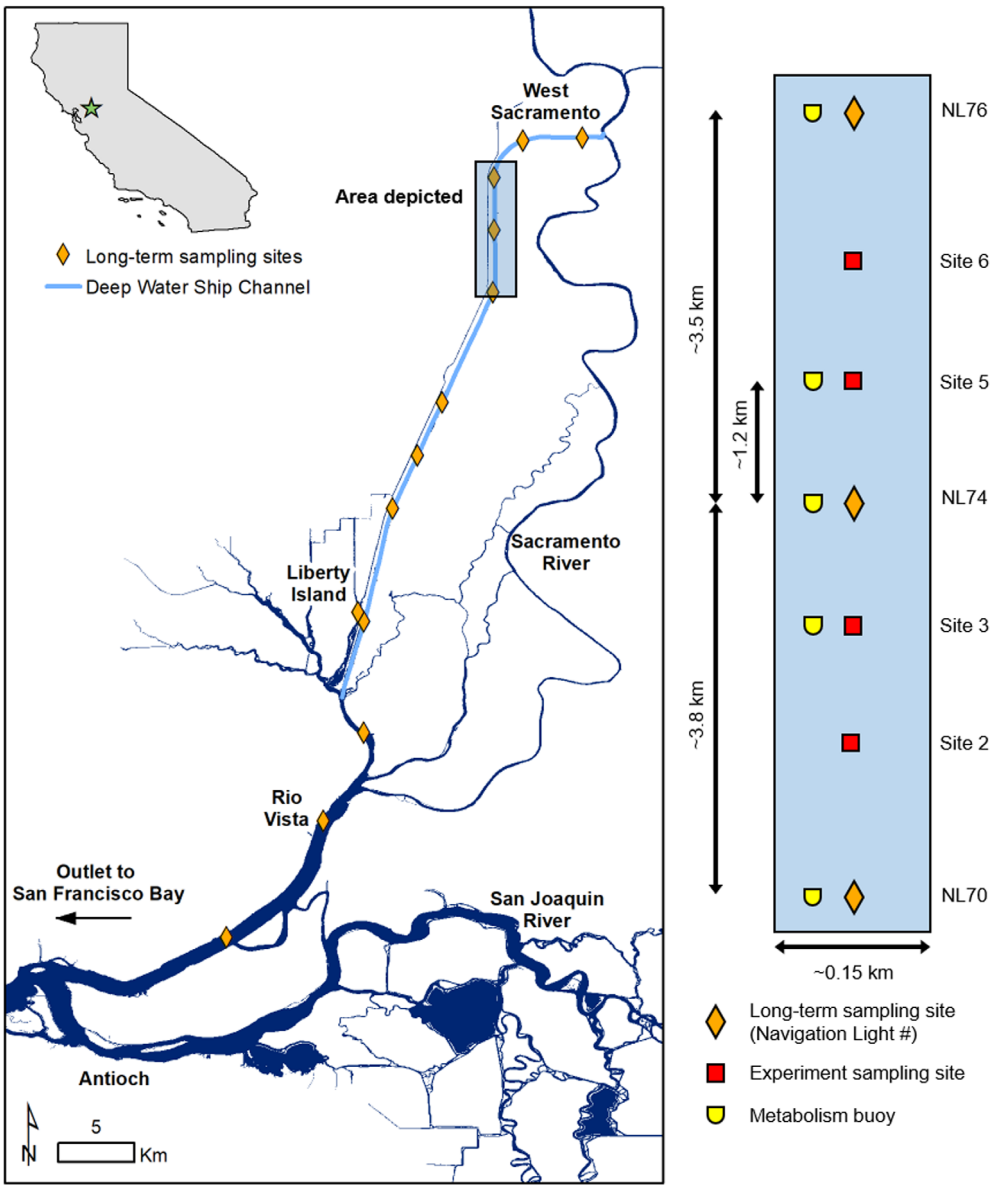

Fig 1. Sacramento River Deep Water Ship Channel sampling and buoy locations. Sensor arrays were deployed on buoys (yellow half circles) ~ 30 m from the western shore. Synoptic sampling occurred in the center of the channel at seven sites (orange diamonds and red squares) evenly spaced longitudinally. Three of the sites are located at Navigation Lights (NL), which are part of a long-term sampling program. Note the inset not drawn to scale.

Metabolism data sources

In summer 2019, a whole-ecosystem experiment was conducted in the DWSC to evaluate the effects of nitrogen fertilization on primary production and food web dynamics. Between 22 July 2019 and 08 August 2019, 1687 kg N (as calcium nitrate—YaharaLiva—Yara, Tampa, Florida) was uniformly applied from a crop dusting airplane to a ~ 60,000 m^2 area in the upper DWSC. Fertilization of the same tidally referenced location occurred on eight dates, and because of advection/dispersion, each day's fertilized area expanded in size and nitrate concentrations returned to background conditions within a few days. The hydrodynamics of the DWSC and ecosystem response to the experiment will be presented elsewhere.

As part of our analysis, a number of ecosystem attributes were monitored at seven sites evenly spaced (~ 1.2 km) in the upper DWSC (Fig. 1). Sensor data and water samples used in metabolism calculations were obtained in the morning (08:00 to 12:00 Pacific Daylight Time (PDT)) on 27 dates between 08 July 2019 and 26 August 2019. Vertical profiles of water temperature, DO, and turbidity were measured on a YSI EXO2 sonde (Xylem, White Plains, New York). On calm days, light extinction was calculated using vertical profiles of photosynthetically active radiation (PAR; LI-1500 Light Sensor Logger,

LI-COR Bioscience, Lincoln, Nebraska). Because light profiles were not collected each day, light extinction for each sample was modeled using turbidity and linear regression (Fig. 2).

On 14 dates (twice weekly), 6 L of surface water (1-m depth) was collected from each site for laboratory incubations. Water was sieved through a 150-μM screen to remove zooplankton and collected in low-density polyethylene cubitainers. Incubation water was stored at ambient temperature in a dark cooler until processing within 8 h of collection.

On 16 dates (~ twice weekly), water samples were collected for ^{18}O analyses. Bubble-free water used in DO isotope ($\delta^{18}O$—O_2) analysis was collected in new 12-mL exetainers that were pre-evacuated and pretreated with 10 μL of water saturated with $HgCl_2$. Exetainers were filled by opening them ~ 0.1 m below the water surface. Samples for water isotopes ($\delta^{18}O$—H_2O and δ^2H—H_2O) were collected in 2-mL glass vials. Vials for water isotopes were overfilled for ~ 15 s using a peristaltic pump and capped without headspace. ^{18}O samples were immediately stored on ice, transferred to a 4°C refrigerator within 6 h of collection, and analyzed within 5 months. Exetainers for $\delta^{18}O$—O_2 were processed at the University of Washington Facility for Compound-Specific Isotope Analysis of Environmental Samples (http://depts.washington.edu/csia/) using a ThermoFinnigan Delta V Plus isotope ratio mass spectrometer in continuous-flow mode connected to a custom autosampler interface (Barth et al. 2004; Holtgrieve et al. 2010). Atmospheric air was used as the working standard, and $\delta^{18}O$—O_2 were corrected based on the mass of ^{16}O—O_2. Vials for $\delta^{18}O$—H_2O and δ^2H—H_2O were analyzed at the Stable Isotope Facility at the University of California-Davis (https://stableisotopefacility.ucdavis.edu/) using a laser water isotope analyzer. Stable isotopic composition of oxygen and hydrogen are reported in the text using delta (δ) notation:

$$\delta^{18}O \text{ or } \delta^2H\,(‰) = \left(\left(\frac{R_{sample}}{R_{standard}}\right) - 1\right) \times 1000, \quad (1)$$

where R_{sample} and $R_{standard}$ are ratios of heavy to light isotopes (^{18}O:^{16}O or ^2H:^1H) in samples and Vienna Standard Mean Ocean Water, respectively.

In addition to boat-based sampling, a network of stationary sensor arrays was deployed to continually monitor vertical dynamics of DO, temperature, and conductivity. Five buoy arrays were anchored in 6–8 m water ~ 30 m offshore at five of the seven boat-based sampling sites (Fig. 1). Each array included three optical DO loggers (PME minidot, DO, and temperature resolution of 0.01 mg L^{-1} and 0.01°C) positioned at depths of 1, 2.5, and 4 m that were attached to cable held vertically. Three temperature (Onset Hobo U22s, temperature resolution 0.02°C) loggers were positioned at 1.5-, 3-, and 4.5-m depths, and three conductivity loggers (Onset Hobo U24s conductivity and temperature resolutions of 0.01°C and 1 μS cm^{-1}) were positioned at 0.5-, 2-, and 3.5-m depths. The DO sensors logged every 5 min, and the temperature and conductivity loggers every 10 min. The pelagic arrays were deployed from 02 July 2019 to 18 September 2019; sensors were cleaned every 2 weeks.

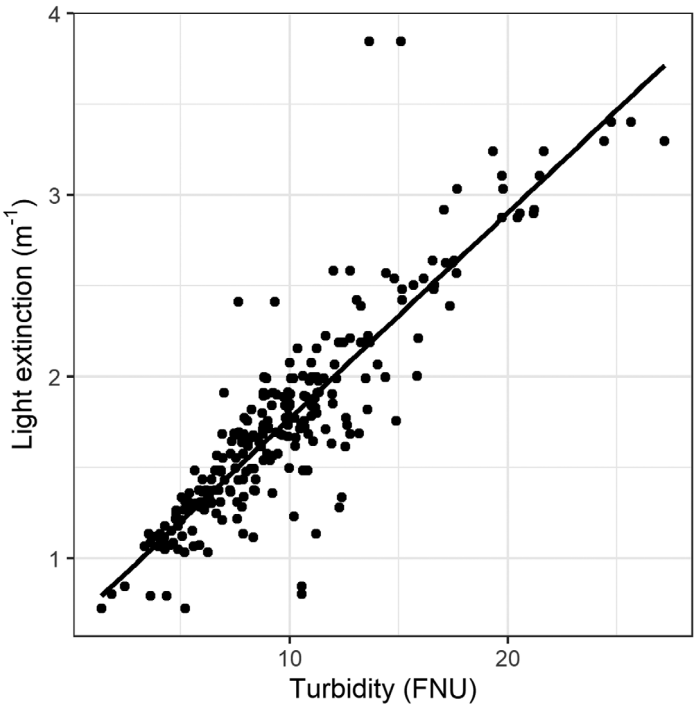

Fig 2. Light extinction coefficient vs. turbidity. Light extinction calculated for 250 light profiles during the study. Turbidity is measured in Formazin Nephelometric Units (FNU). Solid line is the simple linear regression model (df = 248, $p < 0.001$, $R^2 = 0.78$, intercept = 0.635, slope = 0.113) used to predict light extinction based on turbidity.

Metabolism methods

We estimated GPP, ER, and NEP using three independent approaches: laboratory bottle incubations, continuous in situ buoy DO measurements, and a steady-state ^{18}O isotope model. Each method has unique assumptions, and calculations represent different spatial and temporal scales (Table 1). For example, GPP estimates from laboratory incubations represent an instantaneous rate from the photic zone during the day. The incubation method only captures pelagic processes at the time of sampling, while the other approaches incorporate both pelagic and benthic metabolism over the entire day. The in situ buoy approach assumes zero advection and homogeneous conditions spatially across the metabolic footprint. The ^{18}O method assumes steady-state DO dynamics and reflects metabolism and gas exchange over a preceding interval of time (~3 d) depending on the turnover rate of DO (Bogard et al. 2017). All methods require scaling measurements, relying on simplification of physical and biological processes within the channel, but collectively they provide a holistic perspective of metabolism in a spatially heterogeneous and dynamic waterbody.

Table 1. Comparison of rate estimates, data requirements, and underlying principles of metabolism estimation methods.

Method	In situ buoy ($n = 381$)	Laboratory incubation ($n = 98$)	Oxygen isotope ($n = 112$)
		Mean rate ± SD (coefficient of variation)	
GPP	4.95 ± 3.04 (0.61)	3.31 ± 0.90 (0.27)	4.28 ± 0.64 (0.15)
ER	−6.40 ± 3.31 (0.52)	−3.91 ± 0.60 (0.15)	−5.21 ± 0.68 (0.13)
NEP	−1.28 ± 2.13	−0.61 ± 0.62	−0.94 ± 0.96
Primary data	In situ continuous DO at one or more depths	ΔDO in water incubated under varying light and environmental conditions	DO, $\delta^{18}O$—O_2, $\delta^{18}O$—H_2O
Ancillary data	Mixed layer depth Gas transfer velocity	PAR Light extinction	Mixed layer depth Gas transfer velocity Fractionation factors
Limitations	Cannot resolve horizontal or vertical water movements. May need a sensor network or to average temporally to account for spatial heterogeneity and tidal phases	Single point in space and time. Missing benthic and littoral processes. Reliant on scaling rates to the ecosystem	Integrated rate over complex scale. Reliant on physical and isotopic models. Additional considerations in stratified or nonpelagic-dominated systems
Temporal and spatial scales	Daily integrated rate over water footprint. Relates to morphometry, tides, advection, and dispersion	Potential pelagic rate for a single point in space and moment in time	Integrated rate over previous DO turnover timescale, which relates to gas exchange and morphometry. Spatial scale relates to water footprint over time scale
Principle components of uncertainty	Mixing of heterogeneous water sources. Accurate measurement of vertically integrated DO signal. Tidally driven changes in water height and volume	Scaling up to ecosystem, accounting for environmental variation in incubations	Scaling up from a single sample (similar as incubation). Steady-state model assumptions. Lack of validation data. Only appropriate in systems matching physical requirements of the model (well mixed, deep, pelagic-dominated, homogeneous)

Note: Rates for gross primary production (GPP), ecosystem respiratio (ER), and net ecosystem production (NEP) are in grams oxygen per meter squared per day (g O_2 m^{-2} d^{-1}).
n, indicates number of estimates; DO, dissolved oxygen; ΔDO, change in DO over time; δ18O-O_2, isotopic composition of DO; δ18O-H_2O, isotopic composition of water oxygen; PAR, photosynthetically active radiation.

Laboratory incubations

We estimated metabolic rates using repeat DO measurements in water exposed to varying light treatments in an environmental growth chamber. After each sampling campaign, we poured water from each site into nine 500-mL glass jars (three light treatments and three replicates per treatment) that contained a glass marble (to aid in mixing) and a PreSens oxygen sensor spot installed on the interior glass surface (https://www.presens.de/). The sensors transmit data optically, allowing contactless and nondestructive DO measurement without opening the jar. We filled and capped each jar without headspace and placed jars on their sides below an array of metal halide and high-pressure sodium lights in a Conviron growth chamber (https://www.conviron.com/). We created three light treatments by draping shade cloth over two thirds of the jars. We measured light transmission using a Licor PAR meter and the light intensity reaching each group was ~ 885–960 (100% light), 260–285 (30% light), and 75–91 (10% light) μmol m^{-2} s^{-1}. The growth chamber maintained a constant 23°C, which was near ambient conditions in the DWSC. Jars were placed in the chamber within 8 h of collection (~ 16:00 PDT). The jars were allowed to equilibrate overnight in the incubator with lights off, and the first DO measurement was recorded the following morning (~ 08:00 PDT). We then turned on the lights and allowed the jars to incubate for 8–12 h before measuring DO in the afternoon (~ 17:00 PDT). Respiration was measured in each jar immediately following the light incubations, so the respiratory signal reflected autotrophic and heterotrophic activity associated with the prior period of production. Jars were incubated in the dark overnight for ~ 12 h until the final measurement was made (~ 08:00 PDT, approximately 48 h after water was collected). Before each DO measurement, the jars were shaken by hand for at least 15 s to homogenize the contents. We

conducted incubations twice per week because each required ~ 48 h from water sampling to termination.

We used a mass balance method to calculate metabolic rates in each jar. Because the jars were never opened, volumetric rates of NEP, ER, and GPP can be calculated as follows:

$$\mathrm{NEP_{jar}} = \Delta \mathrm{DO_{light}} \div \Delta t, \quad (2)$$

$$\mathrm{ER_{jar}} = \Delta \mathrm{DO_{dark}} \div \Delta t, \quad (3)$$

$$\mathrm{GPP_{jar}} = \mathrm{NEP_{jar}} - \mathrm{ER_{jar}}. \quad (4)$$

$\mathrm{NEP_{jar}}$ is the change in DO concentration (ΔDO) over time (t) during the light period, and $\mathrm{ER_{jar}}$ is the ΔDO over t during the dark period. If we assume ER is independent of light, $\mathrm{GPP_{jar}}$ can be calculated through subtraction. $\mathrm{NEP_{jar}}$, $\mathrm{ER_{jar}}$, and $\mathrm{GPP_{jar}}$ share a common volumetric unit (mg O_2 L^{-1} d^{-1}). Note that $\mathrm{ER_{jar}}$ is typically negative, so $\mathrm{GPP_{jar}}$ should be positive and greater than $\mathrm{NEP_{jar}}$.

We scaled jar rates to daily, vertically integrated ecosystem metabolic rates in the DWSC using solar radiation from the Dixon, CA California Irrigation Management Information System (CIMIS IDs 121; https://cimis.water.ca.gov/) weather station located 25 km SW of the study area, modeled light attenuation in the water column (Fig. 2), and bathymetry. Essentially, the average metabolic rates from each light treatment represented depths and durations exposed to that amount of light. Solar radiation (W m^{-2}) was converted to PAR (μmol m^{-2} s^{-1}) using the R package LakeMetabolizer (Britton & Dodd, 1976; Winslow et al., 2016). At 5-min timesteps (t), we modeled the vertical light field at each site using PAR and the light extinction coefficient. We calculated the depth (Z) and volume (V) of four depth strata (s), separated at light levels of 600, 175, and 20 μmol m^{-2} s^{-1}. These light levels are the approximate midpoints among the incubation light treatments. We integrated volumes of each strata through time, producing the volume–time weights for each jar metabolic rate. In this respect, jars incubated at the 100% light level (900 μmol m^{-2} s^{-1}) represented the uppermost portion of the water column when and where incident light was greater than 600 μmol m^{-2} s^{-1}. For the deepest strata ($s = 4$, <20 μmol m^{-2} s^{-1}; <1% of maximum incident light), we assumed GPP was zero and used $\mathrm{ER_{Jar}}$ from the lowest light treatment ($\mathrm{ER_3}$). To estimate daily, vertically integrated GPP ($\mathrm{GPP_{24h}}$), we summed the volume-time weighted $\mathrm{GPP_{jar}}$ rates. For daily ER ($\mathrm{ER_{24h}}$), we performed a similar calculation, but we doubled the volume–time weighting for the upper three depth strata to account for ER during the night in the portion of the water column that had been illuminated during the day (left side of Eq. 6). We then used subtraction and the total volume (V_{total}) to calculate the weighting for ER from the aphotic zone (right side of Eq. 6). Daily NEP ($\mathrm{NEP_{24h}}$) was calculated through addition.

$$\mathrm{GPP_{24h}} = \sum_{s=1}^{4}\left(\mathrm{GPP}_s \sum_{t=1}^{288} V_{st}\right), \quad (5)$$

$$\mathrm{ER_{24h}} = 2 \times \sum_{s=1}^{3}\left(\mathrm{ER}_s \sum_{t=1}^{288} V_{st}\right) + \mathrm{ER_3} \times \left(V_{\mathrm{total}} - 2 \times \sum_{s=1}^{3}\sum_{t=1}^{288} V_{st}\right), \quad (6)$$

$$\mathrm{NEP_{24h}} = \mathrm{GPP_{24h}} + \mathrm{ER_{24h}}. \quad (7)$$

Total mass rates (g O_2 d^{-1}) were converted to areal rates by dividing by surface area. We use this oversimplification of the water column through time to convert incubation rates to a common unit (g O_2 m^{-2} d^{-1}) for methodological comparison.

In situ buoys

We estimated whole-ecosystem GPP, ER, and NEP using continuous DO measurements and a modified mass balance approach. This technique was pioneered by Odum (1956) and has since been used extensively in studies of aquatic ecosystems (Staehr et al. 2010; Hoellein et al. 2013; Bernhardt et al. 2018). Using the continuous DO measurements from multiple depths, we calculated vertically weighted DO concentration for each buoy at 15-min intervals. We divided the water column into three depth strata (one for each DO sensor) at the midpoint between sensors (1.75 and 3.25 m). We accounted for tidally driven changes in water depth and at each timepoint calculated the volume of each depth strata. Weighting each DO measurement by volume, we calculated a vertically weighted DO concentration (Sadro et al. 2011).

In addition to metabolism, changes in DO result from gas exchange with the atmosphere. Gas exchange was modeled at 15-min intervals using DO concentration, temperature, and specific conductivity from the uppermost sensors and a gas transfer velocity (k) model based on water-side frictional velocity (u^*) (Esters et al. 2017). Wind data from the Dixon, CA CIMIS weather station (CIMIS IDs 121) were used to calculate u^* using the MATLAB "air–sea" package (https://github.com/sea-mat/air-sea) described in Pawlowicz et al. (2001). We estimated k for carbon dioxide (k_{CO2}) using u^* and equations listed in Esters et al. (2017), which we converted to k_{O2} using Schmidt numbers found in Jähne et al. (1987) and Vachon et al. (2010) and temperature dependence models in Raymond et al. (2012). We calculated the equilibrium saturation concentration of DO at the surface using temperature, specific conductivity, and the R package LakeMetabolizer (Winslow et al. 2016). The concentration gradient (i.e., the difference between equilibrium and observed DO concentrations at 1 m depth) was multiplied by k_{O2} to estimate gas exchange at each timestep.

We modeled free-water metabolism using the bookkeeping method (Caffrey 2004) after modifying subroutines in LakeMetabolizer (Winslow et al. 2016). Although there are more computationally sophisticated metabolism models (Winslow et al. 2016; Appling et al. 2018), we chose to use the

bookkeeping model for its simplicity and its inherent sensitivity to spatial and temporal variability (Tassone and Bukaveckas 2019). This model has biases and assumptions (Staehr et al. 2010), but they are consistent through time and among sites. After accounting for gas exchange based on surface DO concentration, changes in vertically weighted DO were used to calculate NEP at each timestep. NEP at night was assumed to equal ER. ER was subtracted from daytime NEP to calculate GPP. We used solar energy data from the CIMIS station (#121) to identify day periods. Periods with PAR > 20 μmol m^{-2} s^{-1} were noted as day, whereas periods after noon with PAR < 20 μmol m^{-2} s^{-1} were noted as night for ER calculations. We summed GPP, ER, and NEP over each dawn-to-dawn 24-h period to calculate daily volumetric rates. We multiplied each by mean water depth over the 24-h period to convert to aerial rates. In total, buoys were deployed for 2.5 months, and after data quality control, we calculated daily metabolism on 69–77 d at the five buoy sites.

We explored two smoothing techniques to account for tidal advection and model error in buoy-based metabolism estimates. First, we calculated rolling averages of daily GPP over 3, 7, and 13 d. Temporal averaging may reduce model error associated with the rigid start/stop times used in the bookkeeping routine that incorrectly attribute DO dynamics to the preceding/following day. Averaging over 13 d (~ half the spring-neap period) would provide a weighted estimate over a spatially balanced metabolic footprint because it would include DO dynamics across the full distribution solar-tidal phasing (Nidzieko et al. 2014). Metabolism was also calculated after tidally filtering the DO time series at each site. Each vertically weighted DO time series was tidal filtered using the WtRegDO R package (https://github.com/fawda123/WtRegDO) and routines described in Beck et al. (2015). This approach uses weighted regression to smooth the DO time series based on day of year, time of day, and tide height, allowing the tidal and biological components of the DO time series to be separated. We used the half-window widths of 3 d, 1 h, and 0.6 m to weight DO observations. After tidally smoothing the DO time series, we used the same bookkeeping routine to estimate daily rates of GPP, ER, and NEP.

Oxygen isotopes

Finally, we modeled metabolism using an isotopic approach that is described in detail in Bogard et al. (2017). The ^{18}O method uses a single measurement of DO, $\delta^{18}O—O_2$, and $\delta^{18}O—H_2O$ to approximate whole-ecosystem metabolic balance. The underlying principle of this approach is that ER, GPP, and gas exchange all change the DO concentration and its isotopic signature (Venkiteswaran et al. 2007). ER lowers DO and fractionates it leaving a heavier DO pool (increases $\delta^{18}O—O_2$). GPP has an opposing effect, as it increases DO and causes the DO pool to become lighter (decreases $\delta^{18}O—O_2$) as the newly formed DO molecules match the isotopic value of water ($\delta^{18}O—H_2O$). In this system, $\delta^{18}O—O_2$ is approximately 22‰ and the average $\delta^{18}O—H_2O$ is −6‰; therefore, GPP will decrease $\delta^{18}O—O_2$. Lastly, exchange with the atmosphere drives the system toward equilibrium in both concentration (100% saturation) and isotopic composition (~ 23.5‰). Note that the effects of GPP, ER, and gas exchange drive DO and $\delta^{18}O—O_2$ along different vectors in the two-dimensional DO:$\delta^{18}O—O_2$ state space (Venkiteswaran et al. 2007), which allows a single sample to approximate all three processes.

While the ^{18}O approach requires minimal sampling for a spatiotemporally integrated rate, it does require several assumptions and estimated model parameters to solve a set of mass balance equations. We used a steady-state ^{18}O metabolism model originally described by Quay et al. (1995) that has been updated and used in other aquatic ecosystem studies (Bocaniov et al. 2012, 2015; Bogard et al. 2017, 2019). Although the model assumes steady-state conditions (neither mixing among adjacent water parcels nor diel DO dynamics), it provides meaningful results in systems that violate these assumptions (Bogard et al. 2019). The same *k* model used in the in situ buoy metabolism method (see above) was used to approximate gas exchange. We used a common respiration fractionation factor (α) for all calculations. We chose an α of 0.98 from Bogard et al. (2017) because it aligns with expectations for systems with greater influence of pelagic processes on ER compared to benthic processes (Hotchkiss and Hall 2014). Although we lack true knowledge of α in this system, we argue that using a common fractionation factor across this study is valid given the proximity of sampling sites, the relative homogeneity among them, and the dominance of pelagic respiration in a deep, well-mixed system. Because we did not analyze water isotopes for every sampling event, we calculated the average for each site. Among all samples, $\delta^{18}O—H_2O$ ranged from −7.7 to −7.1‰, which was much less variable than the range in $\delta^{18}O—O_2$ (17.4 to 23.4‰). The ^{18}O method is most applicable to low-evasion, unstratified, and deep systems where pelagic processes contribute the majority of the metabolic signal (Bogard et al. 2017). The DWSC has all of these features, and samples were collected in the morning prior to daily stratification occurrences. Under these assumptions, we can compare estimates among different sites and times to evaluate the spatial and temporal dynamics of the DWSC as it responds to changes in nutrients and other environmental conditions.

Assessment

Laboratory incubations

When scaled up to the ecosystem level, the incubation-based method indicated the study reach was net heterotrophic. Averaging across sites and through time, the global mean (± SD) incubation rates for GPP, ER, and NEP were 3.31 (± 0.90), −3.91 (± 0.60), and −0.61 (± 0.62) g O_2 m^{-2} d^{-1}, respectively. The coefficients of variation for GPP and ER were 27% and 15%, respectively (Table 1). The incubation-based

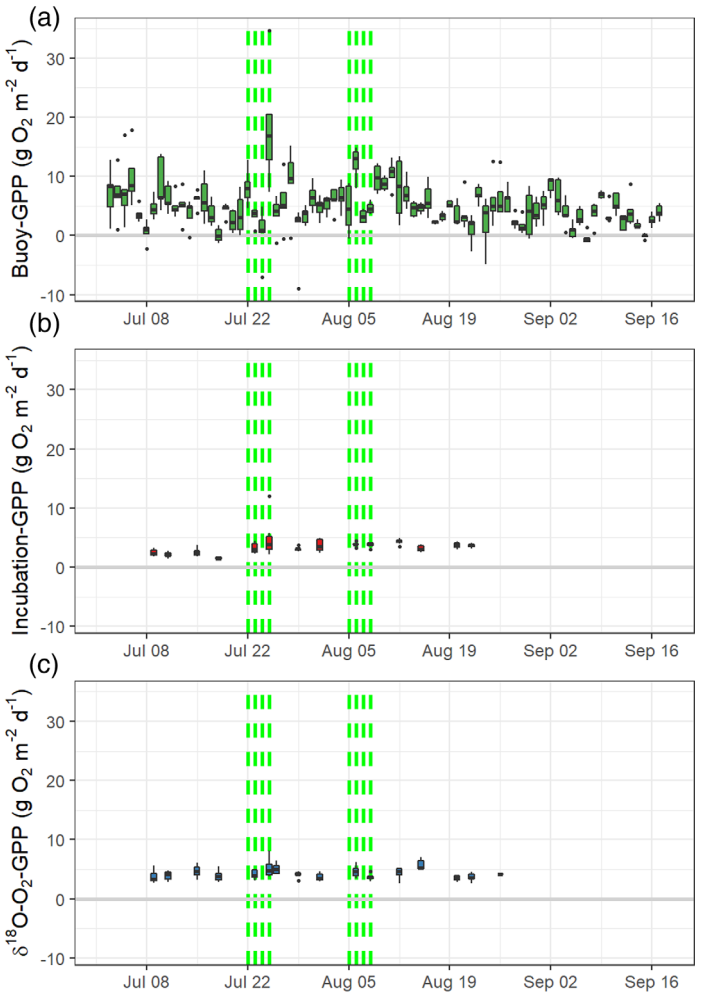

Fig 3. Comparison of gross primary production (GPP) among the in situ buoy (**a**), laboratory incubation (**b**), and oxygen isotope (**c**) methods. Each boxplot is the distribution among sites for daily GPP. The upper and lower edges are the 25th and 75th percentiles, and whiskers are drawn up to 1.5 times the interquartile range. Vertical dashed lines note days calcium nitrate was added to the channel. Metabolic rates are presented in grams oxygen per meter squared per day (g O_2 m^{-2} d^{-1}).

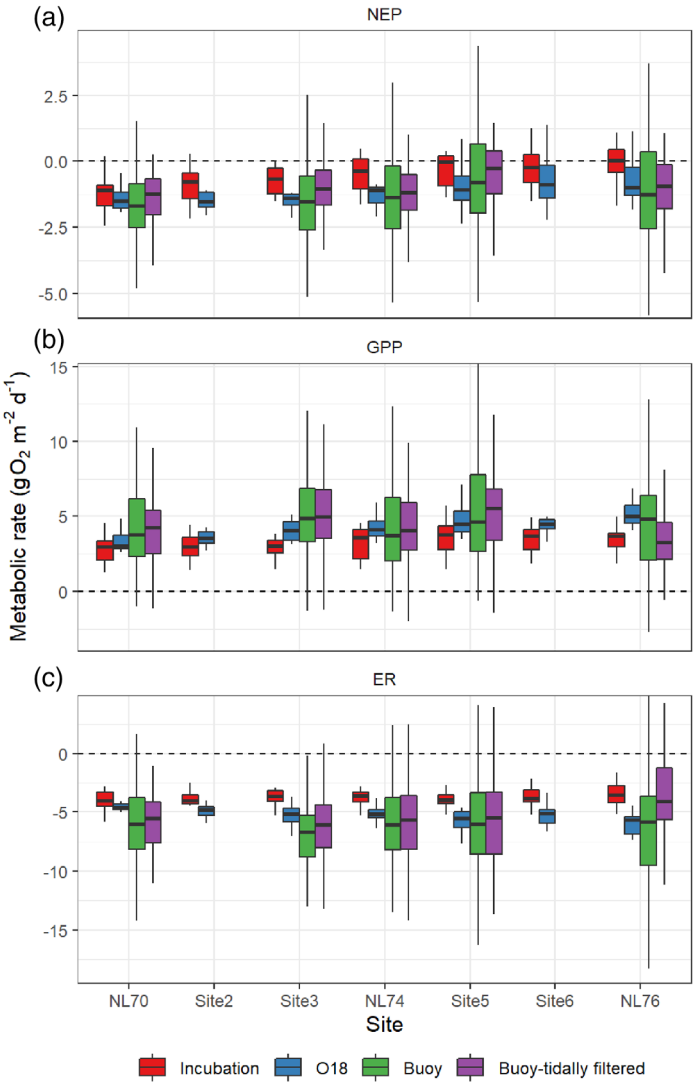

Fig 4. Spatial patterns of net ecosystem production (NEP) (**a**), gross primary production (GPP, **b**) and ecosystem respiration (ER, **c**) among methods. Each box represents the distribution through time at each site. *y*-Axes have been truncated to improve visualization. The upper and lower edges are the 25th and 75th percentiles, and whiskers are drawn up to 1.5 times the interquartile range. Sites are ordered from seaward (NL70) to landward (NL76). Buoys were not deployed at Site2 and Site6. Metabolic rates are presented in grams oxygen per meter squared per day (g O_2 m^{-2} d^{-1}).

rates of GPP, ER, and NEP were on average 48–75% lower (i.e., closer to zero) than the other methods (Table 1) and were consistent through time (Fig. 3b; Supporting Information Fig. S2).

Averaging incubation-based metabolic rates through time highlights clear spatial patterns along the channel's longitudinal axis. The landward sites had higher GPP than the seaward sites (Fig. 4b), aligning with the spatial pattern of turbidity (Feyrer et al. 2017). Because light attenuation was used to scale incubation GPP to the water column, sites with lower turbidity had greater proportions of the water column represented by jars incubated in the higher light treatments. Incubation-based ER did not vary spatially as rates were similar among all sites (Fig. 4c). Combining the spatial patterns of GPP and ER suggest that NEP increased moving landward (Fig. 4a), and median NEP at the uppermost site (NL76) was slightly positive (0.04 g O_2 m^{-2} d^{-1}). Thus, the incubation based approach suggests a gradual switch from net heterotrophy to net autotrophy within the study reach's pelagic zone and the potential for longitudinal transport of organic carbon. However, it must be noted that the incubation rates do not include respiration from the benthic community or organisms > 150 μM.

In situ buoys

In situ buoy-based metabolic rates also indicated the system was net heterotrophic, but metabolic rates were larger in

magnitude and more variable than the other two methods (Fig. 3a; Table 1). Averaging across sites and through time, the global mean buoy rates for GPP, ER, and NEP were 4.95 ($\pm$ 3.04), -6.40 ($\pm$ 3.31), and -1.28 ($\pm$ 2.13) g O_2 m^{-2} d^{-1}, respectively. In contrast to the other methods, there were not clear spatial patterns in buoy-based GPP, NEP, or ER (Fig. 4), in large part because of the high variability. The coefficients of variation for GPP and ER were 61% and 52%, respectively (Table 1), which are over twice that of the incubation method. The higher variability in the buoy rates may reflect sample frequency, as each site had ~ 70 d of buoy-based metabolism in comparison to the incubation and ^{18}O methods. Moreover, the in situ method is known to be more responsive to both short time-scale variations in metabolic rates and physical dynamics affecting DO fluxes within the water column (Caffrey 2004; Staehr et al. 2010; Tassone and Bukaveckas 2019).

There are a number of factors that might affect the high spatial and temporal variability in the buoy metabolic rate measurements, all related to DO dynamics within the water column. The most likely explanation is that our DO measurements were made at too coarse of a vertical resolution for our mass balance model to capture vertical DO dynamics. It is surprising that GPP varied by an order of magnitude among adjacent sites and successive days (Fig. 3a) given that there was no variation in terrestrial inputs, weather during the study period was very consistent, and the sites are hydrologically connected. Rather, we would expect ecosystem metabolism to be autocorrelated in time and space, as has been found in other aquatic systems (Van de Bogert et al. 2012; Solomon et al. 2013; Dodds et al. 2018; Rodríguez-Castillo et al. 2019). It is more plausible that DO dynamics were poorly portrayed in the metabolism model, especially those related to daily water mixing. Despite our prediction that tidal fluxes would result in a homogeneously mixed water column, the water column stratified and de-stratified on most days, temporarily isolating distinct strata within the water column. Over the course of each day, the depth of the upper mixed layer could range over the entire water column (0–8 m). In addition, stratification strength was positively correlated with chlorophyll *a* (Chl *a*) concentrations as well as buoy- and ^{18}O-based rates of GPP (Supporting Information Fig. S3), suggesting that stratification not only contributes to model error, as has been found in lakes (Rose et al. 2014), but also influences phytoplankton dynamics and metabolism. Accurately accounting for highly dynamic vertical mixing requires numerous measurements throughout the water column. As we only measured DO at three depths, and lacked continuous measurements below 4 m, our whole-water-column mass balance may have been poorly resolved with respect to the scale of variation.

Vertically integrated DO concentrations did not always follow a sinusoidal diel pattern, which added uncertainty to metabolism calculations. Overall, the amplitude of the daily DO changes was small, typically less than $\pm$0.4 mg O_2 L^{-1} when scaled to the entire water column. Thus, the metabolic signal was a comparatively small fraction of the total DO mass in the system, and the metabolism model magnified minor inaccuracies in the daily DO budget. We often observed sharp changes in the integrated DO signal and occasional increases at night, which were often associated with episodic stratification and horizontal and (or) vertical mixing. Moreover, depending on the timing of vertical mixing, some portion of a given day's metabolic signal might not be applied to the mass balance until the following day, causing GPP or ER to either be overestimated or underestimated (Staehr et al. 2010; Tassone and Bukaveckas 2019). Thus, daily metabolic rates from other studies with poorly resolved DO monitoring and complex stratification dynamics should be interpreted cautiously due to high uncertainty. However, such directional changes in metabolic signals from mixing or tidal hydrodynamics at the daily time scale often balance out by averaging over longer time periods.

Despite high variability in buoy-based daily estimates, when averaged over longer timescales or after tidally smoothing the DO time series, GPP and ER calculations generally aligned with the other methods (Fig. 4). Others have documented reduced uncertainty in continuous DO-based metabolic rates when averaging over longer timescales (Staehr et al. 2010; Van de Bogert et al. 2012). In other estuary ecosystems, buoy-based metabolic rates may require temporal averaging over longer timescales to account for phase relationships between tidal and solar cycles and spring-neap cycles (Nidzieko et al. 2014). In the DWSC, there are consistently two high tides and two low tides per day, advancing ~ 50 min per day (https://waterdata.usgs.gov/nwis/inventory?agency_code=USGS&site_no=11455095). Averaging daily rates over 13 d (~ half the spring-neap period) would span the full distribution of solar-tidal phases, and thus would integrate across a given location's metabolic footprint. Fortnightly cycles in metabolism estimates may be more apparent in estuaries with greater spatial heterogeneity. For example, the alignment of high tide and high noon can lead to inundation of distinct habitats during times of high productivity, which infrequently contribute to the metabolic signal of a seaward sensor (Nidzieko et al. 2014). In our study, the influence of spatial heterogeneity on the true metabolic signal may be less pronounced due to relatively homogeneous conditions longitudinally in the DWSC. Nonetheless, averaging buoy metabolic rates over fortnightly time scales reduced temporal variability, and the average rates were similar to the ^{18}O method (Fig. 5).

Alternatively, tidally smoothing the DO time series before computing metabolism can be used to account for tidal advection, effectively separating the effects of advection and biology on the observed DO time series (Beck et al. 2015). Tidally filtered rates of GPP were comparable in magnitude to the 3-d rolling average, but with reduced short-term temporal variability (Fig. 5). Tidally smoothing may lead to reduced uncertainty

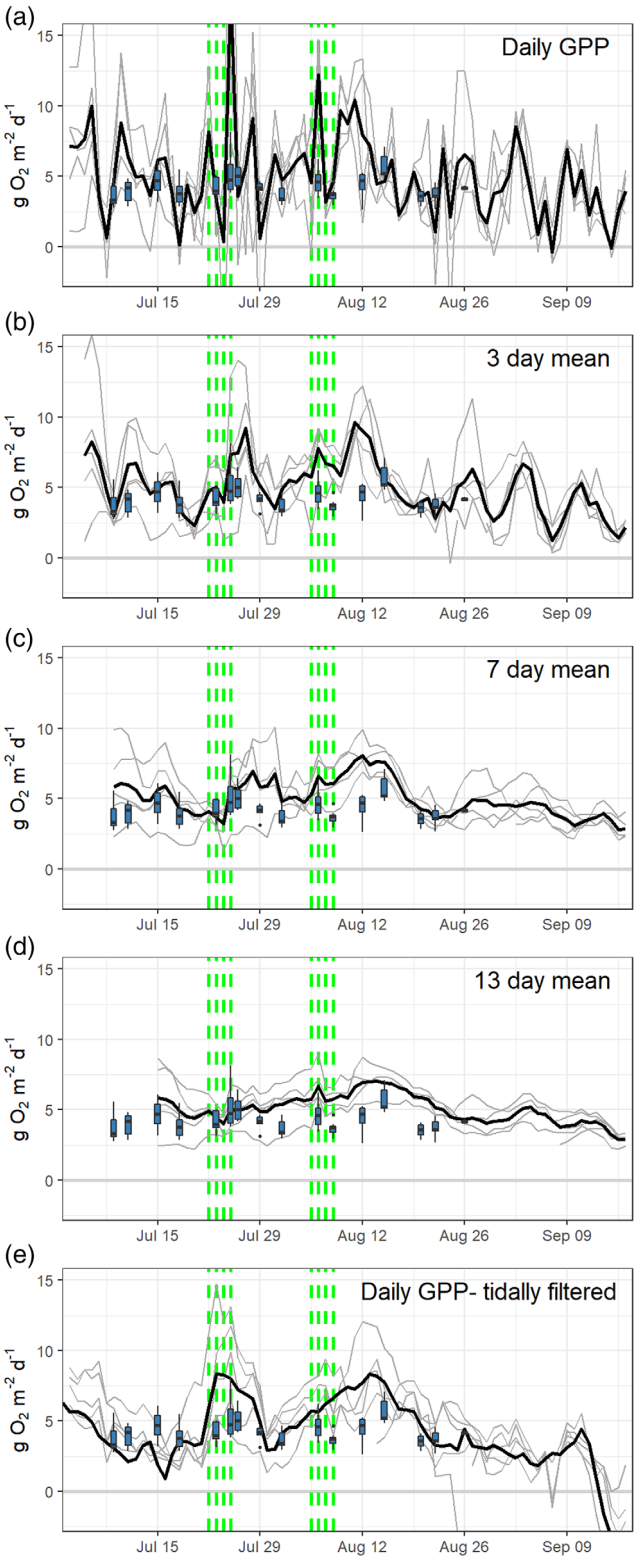

Fig 5. Time series of buoy-based gross primary production (GPP) among rolling window averages (**a**–**d**) and using the tidally filtered dissolved oxygen time series (**e**). Sites are plotted by thin gray lines and the spatial average is the thick black line. Oxygen isotope GPP rates are plotted as blue boxplots (same data as Fig. 3). Metabolic rates are presented in grams oxygen per meter squared per day (g O_2 m^{-2} d^{-1}).

in situations where a single set of sensors is monitoring metabolic activity across vastly different habitats (Kemp and Boynton 1980). In our study, DO at each of the five buoy arrays primarily followed the solar cycle and all stations were highly synchronous (Supporting Information Fig. S4). Furthermore, the cross correlation among the time series did not highlight notable differences in temporal lags among tidal phases and/or distance (Supporting Information Fig. S5), which would indicate relevant tidal advection of DO. In our study reach, there may be minimal benefit to tidally smoothing as the metabolic signal had relatively low tidal distortion (Beck et al. 2015). The weighted regression approach did reduce temporal variability as it uses proximate observations in time, day, and tide. Tidal smoothing is likely more useful in locations with greater spatial heterogeneity, but the approach is not advised on very noisy DO time series or if there is little evidence that the tides are correlated with DO (Beck et al. 2015).

Unlike the other two methods, temporally averaged or tidally filtered in situ rates did not highlight a spatial gradient in metabolism (Fig. 4), which may reflect the higher variability, coarser estimate resolution, or the fact that the metabolic footprints overlap due to advection/dispersion processes. In other parts of the Delta or in other estuaries, temporal averaging or tidally smoothing may be necessary to account for tidal advection and spatial heterogeneity among habitats. We lack confidence in any buoy-based daily estimate, but aggregating rates through time and space provides a more realistic approximation of estuary metabolism across the range of habitats that contribute to the metabolic signal.

Oxygen isotopes

In agreement with the other two methods, the ^{18}O method indicated the study reach was slightly net heterotrophic. Averaging across sites and through time, the global mean ^{18}O-based rates for GPP, ER, and NEP were 4.28 ($\pm$ 0.64), -5.21 ($\pm$ 0.68), and -0.94 ($\pm$ 0.96) g O_2 m^{-2} d^{-1}, respectively. The ^{18}O method had similar coefficients of variation as the incubation-based rates, and the ^{18}O-based rates were between the other two methods (Table 1; Fig. 4). Overall, the three methods suggested similar rates when averaged across the whole study.

The ^{18}O GPP estimates had a clear longitudinal gradient with higher GPP occurring landward in the lower turbidity waters. The ^{18}O method suggested the largest spatial difference in GPP among methods; the uppermost site (NL76) averaged 5.16 g O_2 m^{-2} d^{-1} and the lowest site (NL70) averaged 3.30 g O_2 m^{-2} d^{-1}. Because ER followed a similar but dampened spatial pattern, ranging between -4.56 and -5.91 g O_2 m^{-2} d^{-1}, the resulting NEP spatial pattern was less dramatic than for GPP (Fig. 4). Moving landward, the ^{18}O method suggested that both GPP and ER increase, and the system becomes slightly less heterotrophic with decreasing turbidity. In contrast to the incubation method, the median NEP at all

sites based on ^{18}O was negative suggesting the entire 7-km reach was heterotrophic.

Discussion

Comparisons among methods and scales

Although the spatially and temporally integrated metabolic rates were consistent among methods, notable differences existed when comparing daily calculations. Comparing GPP among methods, the ^{18}O and laboratory incubation estimates had the best agreement (lowest root mean squared error). However, in general, there were poor correlations among methods for GPP (Fig. 6), ER, and NEP (Supporting Information Fig. S1). Some of the disagreements among calculations arise from model uncertainty, as each method has a number of equations and assumptions to scale measurements to the whole ecosystem. While the ^{18}O and in situ buoy methods capture metabolism at the ecosystem level, incubation-based rates exclude benthic communities and organisms larger than 150 μM (e.g., zooplankton). Each method represents a unique community assemblage and horizontal, vertical, and temporal scale (Table 1) contributing to each calculation, thus the three approaches should not necessarily align if true metabolism differs along any temporal or spatial dimension.

In situ buoy-based daily metabolic rates should be reflective of the spatial domain where water originated over the 24-h period. At our central buoy (NL74), complete longitudinal mixing over the median tidal excursion length (2.1 km) typically occurs on the order of a half to full tide cycle (8.4 h). Thus, the spatial scale of the buoy estimates is on the order of 2–5 km but varied with tidal cycles and actual advection/dispersion on that day. Because the DWSC is long and relatively homogeneous, each buoy's metabolic footprint was constrained to the DWSC, and the assumptions regarding consistent ecosystem morphometry are valid. If our buoys were positioned near the channel mouth, the metabolic footprint would include some portion of the greater Delta ecosystem external to the DWSC (Fig. 1), making it challenging to constrain the physical dimensions of the waterbody in the model. Mixing water masses from distinct habitats that vary in depth and biology may cause irregularities in continuous DO signals and metabolism calculations (Kemp and Boynton 1980). Daily metabolism estimates may contain sinusoidal patterns that simply arise from tidal phase relationships that affect the timing and proportions of daily metabolism originating from distinct habitats (Nidzieko et al. 2014; Beck et al. 2015). By arranging sensors within a spatial network, we can more confidently account for tidal advection and achieve a more comprehensive view of metabolism in hydrodynamically complex systems (D'Avanzo et al. 1996).

Laboratory incubation-based rates offer a view of metabolism at a finer spatial and shorter temporal scale than the other two methods. Because water samples were collected from a distinct location and moment in time, in reality these rates reflect the potential metabolic rate of the pelagic zone at that instance. Our samples were collected in the morning, prior to the maximum daily Chl *a* concentration, and the incubations did not reflect in situ changes in phytoplankton over the day that could be effected by production, migration, and (or) grazing dynamics. In the DWSC, Chl *a* concentrations and phytoplankton densities can vary with depth, which is most apparent during stratification. The specific conditions of where and when the incubation sample was collected should be compared to the conditions throughout the rest of the waterbody that the incubation rate represents. Thus, a clear limitation of the incubation method is how to effectively control for environmental variability in the laboratory and scale rates to the ecosystem (Cloern et al. 2014; Murrell et al. 2018). Clearly, continually monitoring Chl *a* and light intensity everywhere in any waterbody is not currently realistic, so the incubation-based method should always be considered cautiously as it only represents one instance in a dynamic and heterogeneous system.

In addition, the incubation approach does not incorporate the metabolism of macrophytes, the littoral zone, zooplankton, and benthic processes. Only pelagic water passed through a 150-μM screen was placed in the incubation jars, and the contributions of other ecosystem communities were not measured. This incubation method will not account for production from littoral vegetation or benthic algae, nor will it include sediment, zooplankton, and fish respiration. In our study, incubation-based GPP and ER were lower than the other two methods on average by a factor of 1.3 to 1.6 (Fig. 4), most likely because the method does not account for benthic respiration nor does it capture periods of higher GPP associated with aggregate phytoplankton biomass or littoral vegetation. The buoy and ^{18}O methods incorporate benthic respiration, which can be of similar magnitude as planktonic respiration in the greater San Francisco Bay ecosystem (Jassby et al. 1993). Subtracting incubation-based ER from the buoy- and ^{18}O-based estimates provides a crude approximation that the incubation approach missed -2.5 and -1.3 O_2 m^{-2} d^{-1} (39% and 25%) of ER, respectively, which was most likely dominated by benthic processes. Overall, we are more confident that the incubation-based GPP represent the potential productivity of the pelagic zone, but due to methodology ecosystem-scaled rates of GPP, ER, and NEP likely underestimate reality.

Lastly, the ^{18}O method reflects a third temporal and spatial scale that blends aspects of the other two methods. Although water samples for the ^{18}O approach are collected at a single moment in time, similar to the incubation method, it represents a much broader spatial and temporal integration of metabolism. The ^{18}O samples include information on the history and mixing of that water parcel, making it reflective over a preceding interval of time. While the exact timescale represented by the ^{18}O method is not an easy calculation, a first order approximation can be made because it is driven

primarily by gas exchange and depth of the surface mixed layer. Over the two-month duration of our study, the average daily k was 1.64 m d^{-1} (range of 0.43–4.34 m d^{-1}). Dividing the average depth (7.5 m) by the average k, implies that DO turnover takes 4.6 d, which is comparable to the timescale that the ^{18}O method encompasses. However, each individual estimate had a different timescale based on the actual rates of k prior to sampling. In addition, this timescale is not equally weighted as the more recent past contributes a larger proportion of that time weighting. Solving for the distribution of time represented by the method can be useful to gain insight into metabolism at finer temporal scales, however for this study sampling occurred 2–4 d apart, and additional assumptions and generalizations are required to investigate finer time scale questions. The spatial scales reflected by the ^{18}O method match the movements of water over the timescale and in this study are on the order of ~ 5 km. Similar to the buoy method, the spatial scale largely reflects advection and dispersion, which varied longitudinally in accordance with variations in tidal excursion lengths and temporally with tidal amplitude and wind.

A number of processes and assumptions over the spatial and temporal scales described above contribute to uncertainty in ^{18}O-based metabolism estimates. Comparatively, the ^{18}O estimates were less variable than the buoy method, likely because the method represented a temporally integrated rate and did not reflect the higher variability inherent in the shorter time scale buoy method. The ^{18}O method identified consistent spatial patterns aligning with the incubation-based approach and the perception of light limitation (Cloern 1987) without using any assumptions about light extinction or water clarity (Table 1). The ^{18}O approach incorporates both pelagic and benthic processes, and it requires less intensive sampling than the other two methods. The physics and ecology of the DWSC (e.g., deep, mixed vertically, pelagic dominated, spatially homogeneous) align with the assumptions needed for the ^{18}O steady-state model (Bogard et al. 2017). Thus, the ^{18}O approach may be a valuable tool to investigate metabolic processes in estuaries or other hydrodynamically complex waterbodies, but only for questions at the appropriate scale and for ecosystems matching the physical constraints of the method.

None of the methods represent true daily metabolism of the DWSC, but collectively provide a complementary assessment of metabolism in a dynamic system. All methods suggested low GPP and ER compared to other estuaries and aquatic systems (Fig. 7; Hoellein et al., 2013), which aligns with the perception that the greater Delta ecosystem has low productivity (Jassby 2008). The absolute difference in GPP among methods was only 1.64 g O_2 m^{-2} d^{-1}, which is small when considering that production in estuary and coastal systems can vary over two orders of magnitude (Hoellein et al. 2013; Nidzieko 2018). The results presented here reflect the typical mid- to late-summer conditions in the DWSC when DIN concentrations are near their annual minimum (< 0.05 mg N L^{-1}), while soluble reactive phosphorus concentrations remain plentiful (~ 0.1 mg P L^{-1}). Temporally, GPP may be greatest in the spring when DIN concentrations are higher, or GPP may follow seasonal patterns in water temperature and solar radiation as has been found in other estuaries (Caffrey et al. 2014; Tassone and Bukaveckas 2019). However, production and CChl a in this 7-km segment over this study appears to be mostly controlled by turbidity and hydrodynamics, which can vary at a range of timescales. Further inquiry into the annual cycle and the contributions from adjacent portions of the DWSC will likely provide a richer context for metabolism in this "relatively simple" portion of the greater Delta ecosystem.

Comments and recommendations

In estuaries, modeling the physical dimensions, hydrodynamics, and biogeochemical dynamics across the metabolic footprint or the entire estuary may be necessary when quantifying metabolic rates (Najjar et al. 2018). For example, in a lagoonal Atlantic estuary, variation in trophic status (heterotrophy vs. autotrophy) among habitat types and locations contributed to near metabolic balance at the estuary scale after considering fluxes and habitat connectivity (Crosswell et al. 2017). Metabolic rates have also been shown to vary along a marsh-dominated estuary's longitudinal axis (Wang et al. 2018), which can manifest as temporal variation at a single location (Nidzieko et al. 2014) and allows spatial decoupling of production and respiration within systems that are highly connected. In our system, both the ^{18}O and incubation calculations suggested a slight gradient in GPP and NEP (Fig. 4), with greater production occurring in the landward DWSC with greater light availability. This spatial heterogeneity, combined with advection and dispersion, allows organic matter produced in one location to fuel respiration elsewhere. As with any metabolic estimate, these calculations should be constrained to spatial extent of the method. Further inquiry across the entire DWSC may reveal nonlinearities as the primary controls (e.g., light, nutrients, flow) alternate and fluxes of material, water, and solutes among adjacent habitats change. Although metabolism estimates based on a limited number of locations are useful to compare systems and investigate drivers (e.g., Caffrey, 2004), within-estuary variability suggests that these spatially limited estimates may not be representative of the estuary as a whole.

We demonstrated that three easily applied and commonly used methods for estimating whole ecosystem metabolism show relatively good agreement in a largely pelagic freshwater tidal estuary, and that emergent insight about ecosystem structure may be gained through a multimethod approach. While the isotope approach provided perhaps the "best" estimate of ecosystem metabolic rates in this study, the degree to which it integrates over space and time may vary considerably

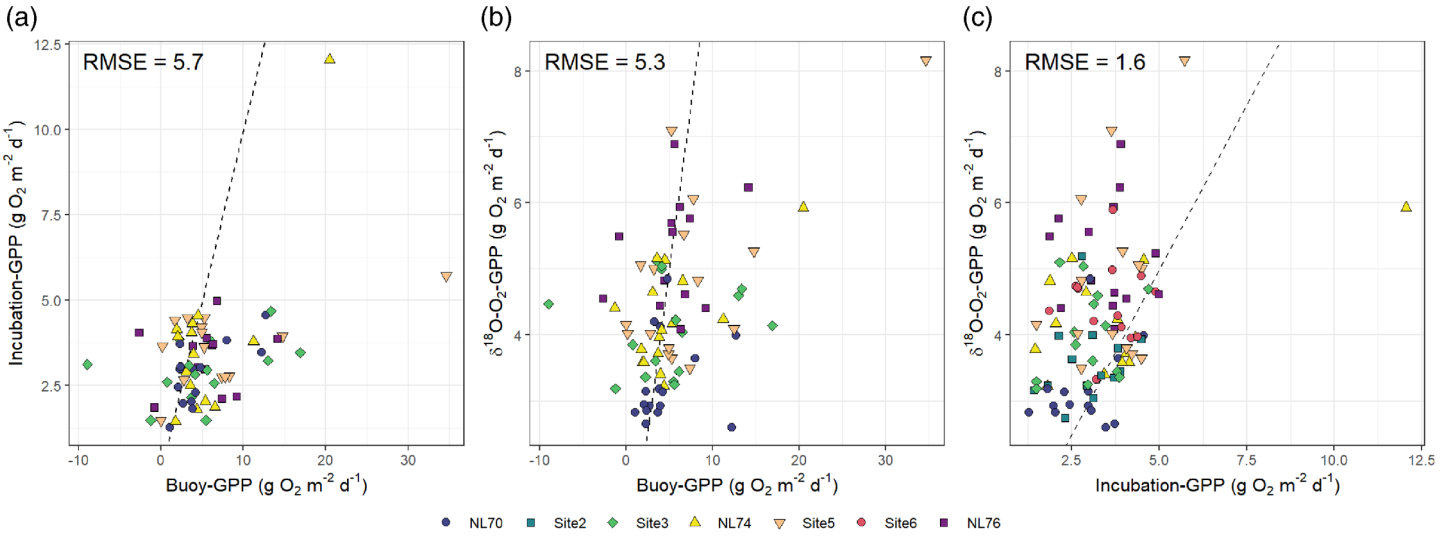

Fig 6. Comparison of daily gross primary production (GPP) among methods. Symbols colored by site from seaward (blue) to landward (purple). Dashed line is the 1 : 1. Metabolic rates are presented in grams oxygen per meter squared per day (g O_2 m^{-2} d^{-1}). RMSE, root mean squared error.

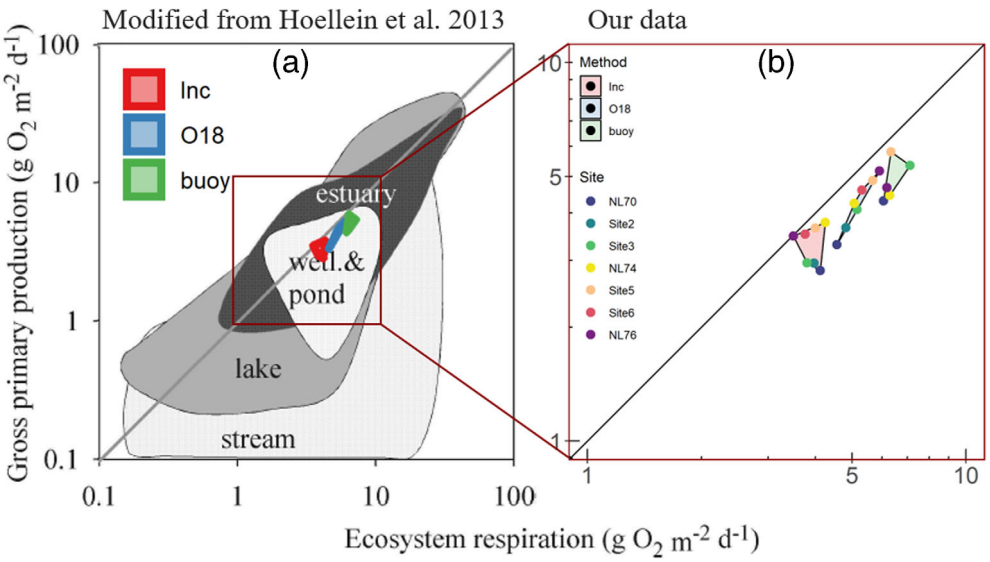

Fig 7. Gross primary production and ecosystem respiration from this study compared with synthesis by Hoellein et al. (2013). Points on the right panel (**b**) are the temporal averages for each site (point color) and the convex hull is colored by method (fill color). Gray polygons of the left panel (**a**) are shaded by aquatic ecosystem type. Points above the 1:1 are net autotrophic; points below are net heterotrophic. Both panels plotted on a log scale. Metabolic rates are presented in grams oxygen per meter squared per day (g O_2 m^{-2} d^{-1}).

within estuaries depending on factors such as morphometry and hydrodynamics. Although the buoy method had the advantage of the highest temporal resolution, it also had considerably higher variability associated with diel variation in hydrodynamics that affect the DO mass balance. Such limitations can be addressed to some extent by averaging over longer timescales (Nidzieko et al. 2014) or tidally correcting the DO time series (Beck et al. 2015), which in this study provided an estimation that was consistent with the other approaches. The ability to continuously monitor metabolic activity using in situ sensors makes their use appealing. However, the resulting data can be noisy and contain artifacts of horizontal (and in this case vertical) advection, which collectively add uncertainty in rate estimates. The incubation approach differed the most from the other two approaches, in large part because it did not reflect benthic processes, nonpelagic autotrophs, zooplankton, nor temporal dynamics in phytoplankton density within the euphotic zone. We suggest the use of multiple concurrent approaches for measuring estuarine ecosystem metabolism better constrains and compartmentalizes

metabolic rate estimates (Murrell et al. 2018) and, when used in comparison with other methods, provides novel insight into complex hydrodynamics and habitat heterogeneity. Estimates using each method should be considered over their specific temporal and spatial scales (Table 1) and likely estimation at multiple locations is needed to fully evaluate the estuary as a whole. Because estuaries are hydrodynamically complex, resolving rates to high precision is unlikely as uncertainty arises from one or more aspects within each method. We are encouraged that we found general agreement among methods when averaging over time and incorporating a spatial network sampling design, which may be even more critical in other estuaries with increased complexity. Accounting for physical mixing, stratification, and spatial heterogeneity in physics and ecology is challenging, but by leveraging multiple methods one can better constrain estuary metabolism.

References

Appling, A. P., R. O. Hall, C. B. Yackulic, and M. Arroita. 2018. Overcoming equifinality: Leveraging long time series for stream metabolism estimation. J. Geophys. Res. Biogeo. **123**: 624–645. doi:10.1002/2017JG004140

Balmer, M., and J. Downing. 2011. Carbon dioxide concentrations in eutrophic lakes: Undersaturation implies atmospheric uptake. Inland Waters **1**: 125–132. doi:10.5268/IW-1.2.366

Barth, J. A. C., A. Tait, and M. Bolshaw. 2004. Automated analyses of 18O/16O ratios in dissolved oxygen from 12-mL water samples. Limnol. Oceanogr. Methods **2**: 35–41. doi:10.4319/lom.2004.2.35

Beck, M. W., J. D. Hagy, and M. C. Murrell. 2015. Improving estimates of ecosystem metabolism by reducing effects of tidal advection on dissolved oxygen time series. Limnol. Oceanogr. Methods **13**: 731–745. doi:10.1002/lom3.10062

Bernhardt, E. S., and others. 2018. The metabolic regimes of flowing waters. Limnol. Oceanogr. **63**: S99–S118. doi:10.1002/lno.10726

Bocaniov, S. A., S. L. Schiff, and R. E. H. Smith. 2012. Plankton metabolism and physical forcing in a productive embayment of a large oligotrophic lake: Insights from stable oxygen isotopes. Freshw. Biol. **57**: 481–496. doi:10.1111/j.1365-2427.2011.02715.x

Bocaniov, S. A., S. L. Schiff, and R. E. H. Smith. 2015. Non steady-state dynamics of stable oxygen isotopes for estimates of metabolic balance in large lakes. J. Gt. Lakes Res. **41**: 719–729. doi:10.1016/j.jglr.2015.05.013

Bogard, M. J., D. Vachon, N. F. St.-Gelais, and P. A. del Giorgio. 2017. Using oxygen stable isotopes to quantify ecosystem metabolism in northern lakes. Biogeochemistry **133**: 347–364. doi:10.1007/s10533-017-0338-5

Bogard, M. J., and others. 2019. Negligible cycling of terrestrial carbon in many lakes of the arid circumpolar landscape. Nat. Geosci. **12**: 180–185. doi:10.1038/s41561-019-0299-5

Bott, T. L., J. T. Brock, C. E. Cushing, S. V. Gregory, D. King, and R. C. Petersen. 1978. A comparison of methods for measuring primary productivity and community respiration in streams. Hydrobiologia **60**: 3–12. doi:10.1007/BF00018681

Britton, C. M. and Dodd, J. D. 1976. Relationships of photosynthetically active radiation and shortwave irradiance. Agric. Meteorol. **17**: 1–7. doi:10.1016/0002-1571(76)90080-7

Caffrey, J. M. 2004. Factors controlling net ecosystem metabolism in U.S. estuaries. Estuaries **27**: 90–101. doi:10.1007/BF02803563

Caffrey, J. M., M. C. Murrell, K. S. Amacker, J. W. Harper, S. Phipps, and M. S. Woodrey. 2014. Seasonal and interannual patterns in primary production, respiration, and net ecosystem metabolism in three estuaries in the Northeast Gulf of Mexico. Estuar. Coasts **37**: 222–241. doi:10.1007/s12237-013-9701-5

Cloern, J. E. 1987. Turbidity as a control on phytoplankton biomass and productivity in estuaries. Cont. Shelf Res. **7**: 1367–1381. doi:10.1016/0278-4343(87)90042-2

Cloern, J. E., S. Q. Foster, and A. E. Kleckner. 2014. Phytoplankton primary production in the world's estuarine-coastal ecosystems. Biogeosciences **11**: 2477–2501. doi:10.5194/bg-11-2477-2014

Cloern, J. E., T. S. Schraga, E. Nejad, and C. Martin. 2020. Nutrient status of San Francisco Bay and its management implications. Estuar. Coasts **43**: 1299–1317. doi:10.1007/s12237-020-00737-w

Cole, J. J., and others. 2007. Plumbing the global carbon cycle: Integrating inland waters into the terrestrial carbon budget. Ecosystems **10**: 172–185. doi:10.1007/s10021-006-9013-8

Crosswell, J. R., and others. 2017. Carbon budget of a shallow, lagoonal estuary: Transformations and source-sink dynamics along the river-estuary-ocean continuum. Limnol. Oceanogr. **62**: S29–S45. doi:10.1002/lno.10631

D'Avanzo, C., J. Kremer, and S. Wainright. 1996. Ecosystem production and respiration in response to eutrophication in shallow temperate estuaries. Mar. Ecol. Prog. Ser. **141**: 263–274. doi:10.3354/meps141263

Demars, B. O. L., J. Thompson, and J. R. Manson. 2015. Stream metabolism and the open diel oxygen method: Principles, practice, and perspectives. Limnol. Oceanogr. Methods **13**: 356–374. doi:10.1002/lom3.10030

Dodds, W. K., and others. 2018. Spatial heterogeneity and controls of ecosystem metabolism in a Great Plains river network. Hydrobiologia **813**: 85–102. doi:10.1007/s10750-018-3516-0

Downing, B. D., B. A. Bergamaschi, C. Kendall, T. E. C. Kraus, K. J. Dennis, J. A. Carter, and T. S. Von Dessonneck. 2016. Using continuous underway isotope measurements to map water residence time in hydrodynamically complex tidal environments. Environ. Sci. Technol. **50**: 13387–13396. doi:10.1021/acs.est.6b05745

Esters, L., S. Landwehr, G. Sutherland, T. G. Bell, K. H. Christensen, E. S. Saltzman, S. D. Miller, and B. Ward. 2017. Parameterizing air–sea gas transfer velocity with dissipation. J. Geophys. Res. Oceans **122**: 3041–3056. doi:10.1002/2016JC012088

Feyrer, F., S. B. Slater, D. E. Portz, D. Odom, T. Morgan-King, and L. R. Brown. 2017. Pelagic nekton abundance and distribution in the Northern Sacramento–San Joaquin Delta. California. Trans. Am. Fish. Soc. **146**: 128–135. doi:10.1080/00028487.2016.1243577

Gaarder, T., and H. H. Gran. 1927. Investigations of the production of plankton in the Oslo Fjord. Rapp. Procès-Verbaux La Réun. **42**: 1–48.

Ganju, N. K., J. M. Testa, S. E. Suttles, and A. L. Aretxabaleta. 2020. Spatiotemporal variability of light attenuation and net ecosystem metabolism in a back-barrier estuary. Ocean Sci. **16**: 593–614. doi:10.5194/os-16-593-2020

Gazeau, F., J.-P. Gattuso, J. J. Middelburg, N. Brion, L.-S. Schiettecatte, M. Frankignoulle, and A. V. Borges. 2005. Planktonic and whole system metabolism in a nutrient-rich estuary (the Scheldt Estuary). Estuaries **28**: 868–883. doi:10.1007/BF02696016

Gerhart, D. Z., and G. E. Likens. 1975. Enrichment experiments for determining nutrient limitation: Four methods compared. Limnol. Oceanogr. **20**: 649–653. doi:10.4319/lo.1975.20.4.0649

Grande, K. D., P. J. L. Williams, J. Marra, D. A. Purdie, K. Heinemann, R. W. Eppley, and M. L. Bender. 1989. Primary production in the North Pacific gyre: A comparison of rates determined by the ^{14}C, O_2 concentration and ^{18}O methods. Deep Sea Res. **36**: 1621–1634. doi:10.1016/0198-0149(89)90063-0

Gross, E., S. Andrews, B. Bergamaschi, B. Downing, R. Holleman, S. Burdick, and J. Durand. 2019. The use of stable isotope-based water age to evaluate a hydrodynamic model. Water **11**(11): 1–17. doi:10.3390/w11112207

Hoellein, T. J., D. A. Bruesewitz, and D. C. Richardson. 2013. Revisiting Odum (1956): A synthesis of aquatic ecosystem metabolism. Limnol. Oceanogr. **58**: 2089–2100. doi:10.4319/lo.2013.58.6.2089

Holtgrieve, G. W., D. E. Schindler, T. A. Branch, and Z. T. A'mar. 2010. Simultaneous quantification of aquatic ecosystem metabolism and reaeration using a Bayesian statistical model of oxygen dynamics. Limnol. Oceanogr. **55**: 1047–1063. doi:10.4319/lo.2010.55.3.1047

Hotchkiss, E. R., and R. O. Hall Jr. 2014. High rates of daytime respiration in three streams: Use of $\delta^{18}OO_2$ and O_2 to model diel ecosystem metabolism. Limnol. Oceanogr. **59**: 798–810. doi:10.4319/lo.2014.59.3.0798

Howard, E. M., A. C. Spivak, J. S. Karolewski, K. M. Gosselin, Z. O. Sandwith, C. C. Manning, and R. H. R. Stanley. 2020. Oxygen and triple oxygen isotope measurements provide different insights into gross oxygen production in a shallow salt marsh pond. Estuar. Coast. **43**: 1908–1922. doi:10.1007/s12237-020-00757-6

Jähne, B., G. Heinz, and W. Dietrich. 1987. Measurement of the diffusion coefficients of sparingly soluble gases in water. J. Geophys. Res. Oceans **92**: 10767–10776. doi:10.1029/JC092iC10p10767

Jassby, A. D., J. E. Cloern, and T. Powell. 1993. Organic carbon sources and sinks in San Francisco Bay: Variability induced by river flow. Mar. Ecol. Prog. Ser. **95**: 39–54. doi:10.3354/meps095039

Jassby, A. D. 2008. Phytoplankton in the upper San Francisco estuary: Recent biomass trends, their causes, and their trophic significance. San Franc. Estuary Watershed Sci. **6**(1): 1–24. doi:10.15447/sfews.2008v6iss1art2

Kemp, W. M., and W. R. Boynton. 1980. Influence of biological and physical processes on dissolved oxygen dynamics in an estuarine system: Implications for measurement of community metabolism. Estuar. Coast. Mar. Sci. **11**: 407–431.

Kemp, W. M., E. M. Smith, M. Marvin-DiPasquale, and W. R. Boynton. 1997. Organic carbon balance and net ecosystem metabolism in Chesapeake Bay. Mar. Ecol. Prog. Ser. **150**: 229–248. doi:10.3354/meps150229

Lindeman, R. L. 1942. The trophic-dynamic aspect of ecology. Ecology **23**: 399–417. doi:10.2307/1930126

Morgan-King, T. L., and D. H. Schoellhamer. 2013. Suspended-sediment flux and retention in a backwater tidal Slough complex near the landward boundary of an estuary. Estuar. Coast. **36**: 300–318. doi:10.1007/s12237-012-9574-z

Murrell, M. C., J. M. Caffrey, D. T. Marcovich, M. W. Beck, B. M. Jarvis, and J. D. Hagy. 2018. Seasonal oxygen dynamics in a warm temperate estuary: Effects of hydrologic variability on measurements of primary production, respiration, and net metabolism. Estuar. Coast. **41**: 690–707. doi:10.1007/s12237-017-0328-9

Najjar, R. G., and others. 2018. Carbon budget of tidal wetlands, estuaries, and shelf waters of Eastern North America. Glob. Biogeochem. Cycl. **32**: 389–416. doi:10.1002/2017GB005790

Nidzieko, N. J. 2018. Allometric scaling of estuarine ecosystem metabolism. Proc. Natl. Acad. Sci. **115**: 6733–6738. doi:10.1073/pnas.1719963115

Nidzieko, N. J., J. A. Needoba, S. G. Monismith, and K. S. Johnson. 2014. Fortnightly tidal modulations affect net community production in a Mesotidal Estuary. Estuar. Coast. **37**: 91–110. doi:10.1007/s12237-013-9765-2

Odum, H. T. 1956. Primary production in flowing waters. Limnol. Oceanogr. **1**: 102–117. doi:10.4319/lo.1956.1.2.0102

Pacheco, F., F. Roland, and J. Downing. 2014. Eutrophication reverses whole-lake carbon budgets. Inland Waters **4**: 41–48. doi:10.5268/IW-4.1.614

Pawlowicz, R., B. Beardsley, S. Lentz, E. Dever, and A. Anis. 2001. Software simplifies air-sea data estimates. Eos Trans. Am. Geophys. Union **82**: 2–2. doi:10.1029/01EO00004

Quay, P. D., D. O. Wilbur, J. E. Richey, A. H. Devol, R. Benner, and B. R. Forsberg. 1995. The ^{18}O: ^{16}O of dissolved oxygen in rivers and lakes in the Amazon Basin: Determining the ratio of respiration to photosynthesis rates in freshwaters. Limnol. Oceanogr. **40**: 718–729. doi:10.4319/lo.1995.40.4.0718

Raymond, P. A., and others. 2012. Scaling the gas transfer velocity and hydraulic geometry in streams and small rivers: Gas transfer velocity and hydraulic geometry. Limnol. Oceanogr. Fluids Environ. **2**: 41–53. doi:10.1215/21573689-1597669

Rodríguez-Castillo, T., E. Estévez, A. M. González-Ferreras, and J. Barquín. 2019. Estimating ecosystem metabolism to Entire River networks. Ecosystems **22**: 892–911. doi:10.1007/s10021-018-0311-8

Rose, K. C., L. A. Winslow, J. S. Read, E. K. Read, C. T. Solomon, R. Adrian, and P. C. Hanson. 2014. Improving the precision of Lake ecosystem metabolism estimates by identifying predictors of model uncertainty: Lake ecosystem metabolism uncertainty. Limnol. Oceanogr. Methods **12**: 303–312. doi:10.4319/lom.2014.12.303

Sadro, S., J. M. Melack, and S. MacIntyre. 2011. Depth-integrated estimates of ecosystem metabolism in a high-elevation lake (Emerald Lake, Sierra Nevada, California). Limnol. Oceanogr. **56**: 1764–1780. doi:10.4319/lo.2011.56.5.1764

Sargent, M. C., and T. S. Austin. 1949. Organic productivity of an Atoll. Eos Trans. Am. Geophys. Union **30**: 245–249. doi:10.1029/TR030i002p00245

Shen, C., J. M. Testa, W. Ni, W.-J. Cai, M. Li, and W. M. Kemp. 2019. Ecosystem metabolism and carbon balance in Chesapeake Bay: A 30-year analysis using a coupled hydrodynamic-biogeochemical model. J. Geophys. Res. Oceans **124**: 6141–6153. doi:10.1029/2019JC015296

Solomon, C. T., and others. 2013. Ecosystem respiration: Drivers of daily variability and background respiration in lakes around the globe. Limnol. Oceanogr. **58**: 849–866. doi:10.4319/lo.2013.58.3.0849

Song, C., W. K. Dodds, M. T. Trentman, J. Rüegg, and F. Ballantyne. 2016. Methods of approximation influence aquatic ecosystem metabolism estimates. Limnol. Oceanogr. Methods **14**: 557–569. doi:10.1002/lom3.10112

Staehr, P. A., D. Bade, M. C. V. de Bogert, G. R. Koch, C. Williamson, P. Hanson, J. J. Cole, and T. Kratz. 2010. Lake metabolism and the diel oxygen technique: State of the science. Limnol. Oceanogr. Methods **8**: 628–644. doi:10.4319/lom.2010.8.0628

Staehr, P. A., J. M. Testa, W. M. Kemp, J. J. Cole, K. Sand-Jensen, and S. V. Smith. 2012. The metabolism of aquatic ecosystems: History, applications, and future challenges. Aquat. Sci. **74**: 15–29. doi:10.1007/s00027-011-0199-2

Staehr, P. A., L. S. Brighenti, M. Honti, J. Christensen, and K. C. Rose. 2016. Global patterns of light saturation and photoinhibition of lake primary production. Inland Waters **6**: 593–607. doi:10.1080/IW-6.4.888

Steemann Nielsen, E. 1952. The use of radio-active carbon (C14) for measuring organic production in the sea. ICES J. Mar. Sci. **18**: 117–140. doi:10.1093/icesjms/18.2.117

Stumpner, P. R., J. R. Burau, and A. L. Forrest. 2020. A Lagrangian-to-Eulerian metric to identify estuarine pelagic habitats. Estuar. Coast. **44**: 1231–1249. doi:10.1007/s12237-020-00861-7

Tassone, S. J., and P. A. Bukaveckas. 2019. Seasonal, interannual, and longitudinal patterns in estuarine metabolism derived from diel oxygen data using multiple computational approaches. Estuar. Coast. **42**: 1032–1051. doi:10.1007/s12237-019-00526-0

Vachon, D., Y. T. Prairie, and J. J. Cole. 2010. The relationship between near-surface turbulence and gas transfer velocity in freshwater systems and its implications for floating chamber measurements of gas exchange. Limnol. Oceanogr. **55**: 1723–1732. doi:10.4319/lo.2010.55.4.1723

Van de Bogert, M. C., D. L. Bade, S. R. Carpenter, J. J. Cole, M. L. Pace, P. C. Hanson, and O. C. Langman. 2012. Spatial heterogeneity strongly affects estimates of ecosystem metabolism in two north temperate lakes. Limnol. Oceanogr. **57**: 1689–1700. doi:10.4319/lo.2012.57.6.1689

Venkiteswaran, J. J., L. I. Wassenaar, and S. L. Schiff. 2007. Dynamics of dissolved oxygen isotopic ratios: A transient model to quantify primary production, community respiration, and air–water exchange in aquatic ecosystems. Oecologia **153**: 385–398. doi:10.1007/s00442-007-0744-9

Wang, S. R., D. Di Iorio, W.-J. Cai, and C. S. Hopkinson. 2018. Inorganic carbon and oxygen dynamics in a marsh-dominated estuary: Inorganic carbon and oxygen dynamics. Limnol. Oceanogr. **63**: 47–71. doi:10.1002/lno.10614

Winslow, L. A., J. A. Zwart, R. D. Batt, H. A. Dugan, R. I. Woolway, J. R. Corman, P. C. Hanson, and J. S. Read. 2016. LakeMetabolizer: An R package for estimating lake metabolism from free-water oxygen using diverse statistical models. Inland Waters **6**: 622–636. doi:10.1080/IW-6.4.883

Yang, B., S. R. Emerson, and S. M. Bushinsky. 2017. Annual net community production in the subtropical Pacific Ocean from in situ oxygen measurements on profiling floats. Global Biogeochem. Cycles **31**: 728–744. doi:10.1002/2016GB005545

Yvon-Durocher, G., J. I. Jones, M. Trimmer, G. Woodward, and J. M. Montoya. 2010. Warming alters the metabolic balance of ecosystems. Philos. Trans. R. Soc. B Biol. Sci. **365**: 2117–2126. doi:10.1098/rstb.2010.0038

Acknowledgments

We thank Laura Benninger, Stuart Angerer, Ian Smith, Nicolas Sakata, and Luke Davis from the U.S. Bureau of Reclamation for assistance with experimental design, field work, and permitting. Thanks to Michael Porter, Catherine Ruhl, Norbert Vandenbranden, Brian Bergamaschi, Elizabeth Stumpner, Bryan Downing, Katy O-Donnell, Thomas Johnston, Kyle

Nakatsuka, Brittany Griffiths, Jim DeRose, Joe Hatfield, Anna Conlen, Henry Rabas, Chris Vallee, and Ryan Johnson from the California Water Science Center for instrumentation, field logistics, and technical guidance. Thanks to Julia Hart, Gordon Holgtrieve, and Matt Bogard for oxygen isotope analysis and modeling. Thanks for Xien Wang, Isabella Glenn, Lindsay Vaughan, Reed Tran, Owen Sowerwine, Chris Dunbar, Colby House, Pao Perez, Neil Singh, Alice Tung, Christine Parisek, Bryan Currinder, Vince Butitta, Nick Framsted, and Andrew Pietersen from UC-Davis for lab and field assistance. We thank two anonymous reviewers, Jordan Read, and Scott Engisn for reviewing the manuscript. Data are available at ScienceBase (https://doi.org/10.5066/P9SKCIUW). Any use of trade, product or firm names is for descriptive purposes only and does not imply endorsement by the U.S. Government.

Submitted 07 January 2021
Revised 30 June 2021
Accepted 19 August 2021

Associate editor: Scott Ensign